

# Generalized Sub-Schawlow-Townes Laser Linewidths Via Material Dispersion

Jason Cornelius Pillay,<sup>1</sup> Yuki Natsume,<sup>1</sup> A. Douglas Stone,<sup>2</sup> and Y. D. Chong<sup>1,3,\*</sup>

<sup>1</sup>*Division of Physics and Applied Physics, School of Physical and Mathematical Sciences, Nanyang Technological University, Singapore 637371, Singapore*

<sup>2</sup>*Department of Applied Physics, Yale University, New Haven, Connecticut 06520*

<sup>3</sup>*Centre for Disruptive Photonic Technologies, Singapore 637371, Singapore*

A recent  $S$  matrix-based theory of the quantum-limited linewidth, which is applicable to general lasers, including spatially non-uniform laser cavities operating above threshold, is analyzed in various limits. For broadband gain, a simple interpretation of the Petermann and bad-cavity factors is presented in terms of geometric relations between the zeros and poles of the  $S$  matrix. When there is substantial dispersion, on the frequency scale of the cavity lifetime, the theory yields a generalization of the bad-cavity factor, which was previously derived for spatially uniform one-dimensional lasers. This effect can lead to sub-Schawlow-Townes linewidths in lasers with very narrow gain widths. We derive a formula for the linewidth in terms of the lasing mode functions, which has accuracy comparable to the previous formula involving the residue of the lasing pole. These results for the quantum-limited linewidth are valid even in the regime of strong line-pulling and spatial hole-burning, where the linewidth cannot be factorized into independent Petermann and bad-cavity factors.

## I. INTRODUCTION

One of the oldest problems in laser physics is the characterization of the quantum-limited laser linewidth. In their seminal paper on the theory of the laser, Schawlow and Townes derived the formula [1]

$$\delta\omega_{\text{ST}} = \frac{\hbar\omega_0\gamma_c^2}{2P}, \quad (1)$$

where  $\omega_0$  is the frequency of the laser mode,  $\gamma_c$  is the linewidth (FWHM) of the corresponding passive cavity resonance, and  $P$  is the output power. Several corrections to this result were found by subsequent researchers: (i) an excess noise factor arising from incomplete population inversion in the gain medium; (ii) the Petermann factor, which describes excess noise due to mode non-orthogonality [2–7]; (iii) the Henry  $\alpha$  factor, which describes indirect phase fluctuations from instantaneous intensity changes caused by spontaneous emission [8]; and (iv) a “bad-cavity” factor which reduces the linewidth when the cavity decay rate is on the order of the gain width [9–14]. The first three factors all broaden the linewidth relative to the basic Schawlow-Townes result, Eq. (1). The bad-cavity factor, however, *reduces* the linewidth. Its origin was originally attributed to the slow-down of phase diffusion caused by atomic memory [9–11]; subsequently, Kuppens *et al.* gave an alternative interpretation based on the increase in the laser cavity’s group refractive index due to the frequency dispersion of the gain medium [13]. This factor deviates significantly from unity in bad-cavity lasers, whose cavity decay rates are on the order of the gain width (or polarization dephasing rate), and has been demonstrated experimentally in

a HeNe gas laser [13, 14]. It has also recently been re-derived in the context of quantum cascade lasers, where it yields a small but measurable correction to the linewidth [20]. Recently, there have been theoretical proposals to achieve ultra-low linewidth lasers by exploiting this effect with superradiant gain media [15–19].

Recently, two of the present authors developed a theory of the quantum-limited laser linewidth [21], based on the properties of the scattering matrix ( $S$  matrix) derived from Steady-state Ab-initio Laser Theory (SALT) [22–25]. According to this theory, the cavity decay rate  $\gamma_c$  in Eq. (1) is replaced by a generalized decay rate

$$\gamma_L = \left| \text{Res}(s) \frac{\Psi_L^\dagger \Psi_L}{\Psi_L^T \Psi_L} \right|, \quad (2)$$

where  $\text{Res}(s)$  denotes the residue of the  $S$  matrix eigenvalue,  $s$ , which diverges at the laser frequency, and  $\Psi_L$  is the corresponding  $S$  matrix eigenvector. Note that  $\Psi_L$  is not the lasing mode function, i.e. it is not the electric field as function of position, but rather an  $N$ -component complex vector, where  $N$  is the number of asymptotic scattering channels coupled to the laser cavity. The quantity denoted  $\Psi_L^\dagger \Psi_L$  is the usual hermitian norm of this vector, which will be set to unity by convention. The quantity  $\Psi_L^T \Psi_L = \sum_{i=1}^N \Psi_{L,i}^2$  is the biorthogonal norm of  $\Psi_L$ , a complex number with modulus less than or equal to unity. It does not represent the Petermann factor,  $K$ , despite its apparent similarity to familiar integral formulas for the same; in fact, for one-port ( $N = 1$ ) lasers,  $|\Psi_L^T \Psi_L| = 1$  even though  $K < 1$ .

SALT describes single- or multi-mode lasing above threshold for arbitrary laser cavities, and the  $S$  matrix used in Eq. (2) is a non-linear  $S$  matrix computed from the SALT equations as described in [21]. It takes into account both the gain competition, spatial hole-burning and self-saturation effects present above threshold. It was shown in Ref. 21 that Eq. (2) incorporates the in-

\* yidong@ntu.edu.sg

complete inversion and Petermann factors, and due to the generality of the  $S$  matrix approach, it can be applied to complex modern laser cavity geometries, such as microdisk, photonic crystal, and random lasers. By contrast, previous derivations of the Petermann factor have been specific to one-dimensional (1D) cavities [2–7], with the notable exception of a paper by Schomerus [26] which will be discussed below.

In this paper, we analyze the  $S$ -matrix linewidth formula further, and derive additional results which flow from it. We show that Eq. (2) also exhibits the bad-cavity linewidth reduction effect mentioned above [9–14]. Before proving this, we analyze a one-port laser (e.g. a Fabry-Pérot single-mode laser), for which the  $S$ -matrix can be completely described in terms of the poles and zeros positions. This leads, in Sections II and III, to a simple geometric interpretation of the Petermann and bad-cavity factors in terms of the motion of the poles and zeros of the  $S$ -matrix in response to the pumping of the gain medium. For more general lasers, including non-1D and/or spatially non-uniform lasers, the full  $S$ -matrix theory allows for a more rigorous calculation of the linewidth. In Section IV, we use the  $S$ -matrix theory to derive an alternative formula for  $\gamma_L$  in terms of the lasing wavefunction, and show that the bad-cavity linewidth reduction factor is automatically incorporated. By contrast, the bad-cavity factor was derived in Refs. 9–11 using Langevin equations, in which the spatial variation of the lasing mode is neglected, and in Ref. 12 using a Green’s function method specific to 1D cavities. For Fabry-Pérot cavities, we show analytically and numerically that our theory reduces to the earlier results. In Section V, we present numerical analyses of more complex lasers, including spatially non-uniform 1D cavities and 2D cavities. When spatial hole-burning and line-pulling (due to the frequency dispersion of the gain medium) are negligible, the  $S$ -matrix theory is in good agreement with previous, more approximate theories, where the bad-cavity factor and Petermann factor are treated as independent quantities. In the presence of strong line-pulling or spatial hole-burning, we find that this factorization breaks down. The deviations in the linewidth predicted by the  $S$ -matrix theory, under these more general conditions, can be tested in future experimental work.

## II. GEOMETRIC VIEW OF THE PETERMANN FACTOR

Possibly the most-studied correction to the Schawlow-Townes linewidth formula is the Petermann factor, which accounts for the fact that the modes of any open system, including laser cavities, are non-orthogonal. When spontaneous emission noise is decomposed into these non-orthogonal modes, there is an excess in the overall noise level associated with noise correlation in different modes [3]. This effect was originally discovered and discussed in the context of transverse modes of gain-guided

lasers [2, 3, 5], and subsequently extended to longitudinal modes by Hamel and Woerdman [4, 6, 7]. The Petermann factor is written as

$$K = \left| \frac{\int dr |\varphi(r)|^2}{\int dr \varphi(r)^2} \right|^2 > 1, \quad (3)$$

where  $\varphi(r)$  is either a transverse or longitudinal wavefunction (mode amplitude), and the integral is, correspondingly, either taken over the area transverse to the axis of the laser cavity or along the axial direction. The methods which have previously been used to derive the Petermann factor [2–7] are limited to 1D lasers with a well-defined axis, and with spatially uniform dielectric functions. In particular, for the longitudinal Petermann factor, Eq. (3) can equivalently be written as

$$K = \left[ \frac{(|r_1| + |r_2|)(1 - |r_1 r_2|)}{2|r_1 r_2| \ln |r_1 r_2|} \right]^2, \quad (4)$$

where  $r_1$  and  $r_2$  are the reflection coefficients at the two ends of the uniform 1D cavity [4, 6]. Recently, Schomerus has derived a generalization of the Petermann factor which applies to sub-threshold high-Q 2D lasers [26]. We will discuss the relationship between our results and those of Schomerus in Section IV.

In this section, we develop a simple and intuitive interpretation of the Petermann factor, based on the analytic properties of the  $S$ -matrix. In the next section, we will see that the bad-cavity linewidth reduction factor also emerges in this picture. The important role of dispersion in reducing the linewidth was noted in Ref. 21, but in a less complete manner, as we did not then appreciate its connection to the bad-cavity factor in Fabry-Pérot systems. The geometric interpretation of the Petermann factor was also touched upon in a recent work on the bandwidth of coherent perfect absorption [27].

We begin by considering a one-port laser, such as a 1D cavity with a perfect mirror on one end, or a higher-dimensional cavity with a single-mode port. In this case,  $S(\omega)$  is a scalar whose exact form depends on the distribution of dielectric and gain material in the system. Under very general conditions [29],  $S(\omega)$  is analytic and possesses an infinite discrete set of poles and zeros in the complex  $\omega$  plane, denoted by  $\{\omega_j^p\}$  and  $\{\omega_j^z\}$  respectively. In a passive cavity (one without material gain or loss), time-reversal symmetry ensures that the poles and zeros are symmetrically placed around the real- $\omega$  axis, allowing us to label them with a single index  $j$  such that  $\omega_j^p = (\omega_j^z)^*$ . For example, Fig. 1(a) shows the poles and zeros for a spatially non-uniform 1D cavity (open symbols). The poles of the passive cavity correspond to scattering resonances, whose decay rates (FWHM) are defined as  $\gamma_j = -2\text{Im}(\omega_j^p)$ .

As gain (and/or loss) is introduced, these labeled poles and zeros move in the complex  $\omega$  plane, as shown in Fig. 1(a). They no longer form conjugate pairs, but if their frequencies  $\{\omega_j^{p,z}\}$  are known, we can compute  $S(\omega)$

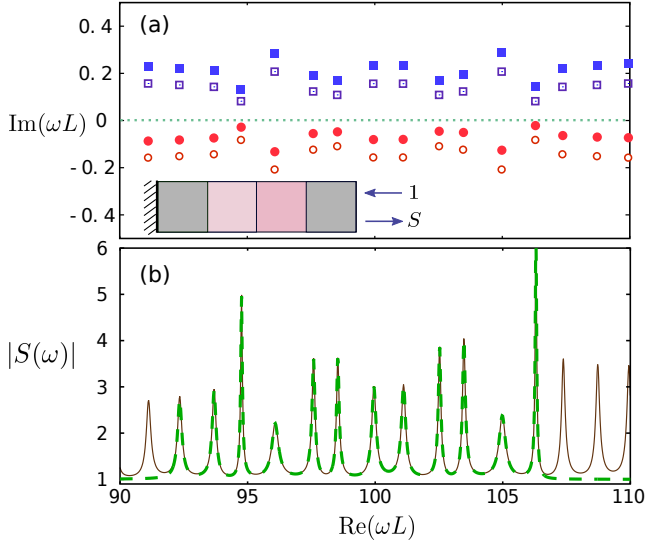


FIG. 1. (color online) (a) Poles and zeros of a one-port 1D cavity, consisting of four slabs of equal length  $L/4$  with a perfect mirror on the left boundary (inset), and  $\epsilon = 1$  in the external region. Filled symbols show poles (circles) and zeros (squares) for frequency-independent slab refractive indices of (left to right)  $n = [3, 1.5 - 0.002i, 2.5 - 0.005i, 3]$ . Open symbols show poles and zeros for the passive cavity, with  $\text{Im}(n) = 0$ . (b) Values of  $S(\omega)$  on the real- $\omega$  line, for the cavity with gain, calculated exactly (solid curve) and using the Padé approximant of Eq. (5) with 12 pole/zero pairs near  $\omega L = 100$  (dashed curve).

for any  $\omega$  using the Padé approximant

$$S(\omega) \simeq \prod_j \frac{\omega - \omega_j^z}{\omega - \omega_j^p}, \quad (5)$$

up to an irrelevant phase factor which has been omitted. For the passive cavity, Eq. (5) gives  $|S(\omega)| = 1$  for all real  $\omega$ , as expected. The precision of the Padé approximant increases as more pole and zero pairs are included in the product. Its validity for  $S(\omega)$  is demonstrated numerically in Fig. 1(b).

A lasing mode corresponds to a pole of  $S(\omega)$  located on the real- $\omega$  axis [25]. As noted, this description holds both at the lasing threshold and above threshold, except that  $S(\omega)$  above threshold must be computed using an  $\omega$ -dependent dielectric function with a non-linear contribution from spatial hole-burning, which can be found via the SALT method [22–25]. Denoting the lasing pole by  $j = 0$ , we can use Eq. (2) with Eq. (5) to obtain the generalized decay rate

$$\gamma_L = |\omega_0^p - \omega_0^z| \prod_{j \neq 0} \left| \frac{\omega_0^p - \omega_j^z}{\omega_0^p - \omega_j^p} \right|. \quad (6)$$

(As mentioned above, for the one-port system, the lasing eigenvector  $\Psi$  has only one component, so  $|\Psi^T \Psi| = 1$ .)

Fig. 1(a) demonstrates the effects of broad-band gain on the poles and zeros. In this case, the gain is simply

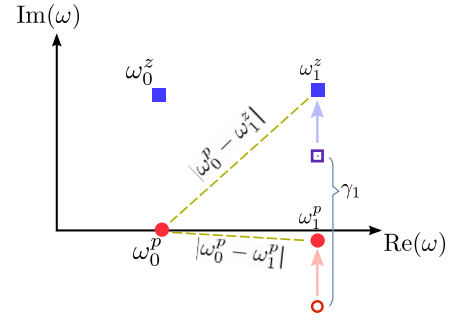


FIG. 2. (color online) Schematic of a pair of neighboring poles and zeros, showing the geometric interpretation of the Petermann factor.  $\omega_0^p$  is a pole which has reached the real- $\omega$  axis. According to Eq. (6), the contribution of the neighboring pole ( $\omega_1^p$ ) and zero ( $\omega_1^z$ ) to the generalized decay rate is the ratio of the lengths of the upper and lower dashed lines, which is  $> 1$ . Open symbols indicate  $\omega_1^{p,z}$  for the passive cavity.

frequency-independent; more generally, “broad-band” gain refers to a gain width much larger than the free spectral range and resonance decay rates. The poles and zeros move almost directly upward in the complex  $\omega$  plane, relative to their passive cavity positions, and each pole and zero in a pair moves by approximately the same amount. In order for a given pole (say  $j = 0$ ) to lase, it must move a distance of  $\gamma_0/2$ ; the corresponding zero moves by the same amount, so the first factor in Eq. (6) is  $|\omega_0^p - \omega_0^z| \approx \gamma_0$ . This factor corresponds to an unmodified Schawlow-Townes linewidth.

Next, consider the product terms in Eq. (6). Neighboring pairs of zeros and poles also move upward from their passive cavity positions. Hence, as indicated in Fig. 2,

$$K_{\text{ansatz}} \equiv \prod_{j \neq 0} \left| \frac{\omega_0^p - \omega_j^z}{\omega_0^p - \omega_j^p} \right|^2 > 1. \quad (7)$$

We interpret  $K_{\text{ansatz}}$  as the Petermann factor. It approaches unity in the limit where the free spectral range is much larger than the resonance decay rates  $\gamma_j$ , in accordance with the usual notion that the Petermann factor is negligible for high  $Q$ .

To show that  $K_{\text{ansatz}}$  is indeed the Petermann factor, suppose our one-port laser is spatially uniform and 1D, with reflection coefficient  $r$  at the output port. The frequencies of the poles and zeros, denoted  $\omega_{p,z}$ , satisfy [28]

$$\exp[\pm 2in\omega_{p,z}L] r = e^{-i\phi}, \quad (8)$$

where  $n$  is the refractive index in the cavity,  $L$  is the cavity length, and  $\phi$  is the phase change at the perfectly reflecting port. For the passive cavity ( $\text{Im}[n] = 0$ ), with frequency-independent  $n$  and  $r$ , Eq. (8) implies that the poles and zeroes are equally spaced with free spectral range  $\Delta\omega$  and located at equal distances  $\gamma_0/2$  from the real axis, where  $\ln|r| = -\pi\gamma_0/\Delta\omega$ . Assuming an “ideal” gain medium which moves all the poles up to the real

axis, and all the zeros up by an equal amount, Eq. (7) implies

$$K_{\text{ansatz}} \simeq \prod_{j \neq 0} \frac{(j\Delta\omega)^2 + \gamma_0^2}{(j\Delta\omega)^2} = \left[ \frac{\Delta\omega}{\pi\gamma_0} \sinh\left(\frac{\pi\gamma_0}{\Delta\omega}\right) \right]^2. \quad (9)$$

In the last equality, we have used Euler's product formula for the sine function,

$$\sin(\pi z) = \pi z \prod_{j=1}^{\infty} \left(1 - \frac{z^2}{j^2}\right), \quad (10)$$

with an imaginary argument. Plugging into Eq. (8) yields

$$K_{\text{ansatz}} \simeq \left| \frac{1 - r^2}{2r \ln|r|} \right|^2. \quad (11)$$

This agrees exactly with Eq. (4), the formula for the longitudinal Petermann factor derived in Refs. 4 and 6, for the one-port case ( $r_1 = r, |r_2| = 1$ ). This link between the motion of  $S$ -matrix poles and zeros and the Eq. (4) is a new result of this paper. This geometric interpretation also emphasizes the fact that the Petermann factor relates to the cavity finesse,  $\Delta\omega/\gamma_0$ , not the  $Q$ -factor  $\omega_0/\gamma_0$ .

For a cavity with more than one port, the ansatz (6) no longer applies since the  $S$ -matrix has more than one eigenvalue. (As an exception, in a two-port parity symmetric system, the eigenspace of  $S$  factorizes and Eq. (6) can be used with only even/odd values of  $j$  in the product.) In the more general case,  $\gamma_L$  would have to be calculated using Eq. (2), or from the wavefunction formula derived in Section IV.

### III. THE BAD-CAVITY FACTOR

In the previous section, when showing that the Padé approximant ansatz (6) for the generalized decay rate yields the Schawlow-Townes-Petermann linewidth for broad-band gain, we assumed that the gain displaces the poles from their passive cavity positions by the same amount as the zeros. Thus, for instance, the leading factor of  $|\omega_0^p - \omega_0^z|$  in Eq. (6) takes the value  $\gamma_0$ . When the dielectric function is frequency dependent, this condition is violated. Consider a Maxwell-Bloch gain medium,

$$\epsilon(\omega) = n_0^2 + \frac{D\gamma_{\perp}}{\omega - \omega_a + i\gamma_{\perp}}, \quad (12)$$

where  $n_0^2$  is the background permittivity,  $D$  a scaled inversion factor proportional to the pump,  $\omega_a$  the polarization resonance frequency, and  $\gamma_{\perp}$  the polarization dephasing rate (gain width) [22–25]. This formula for  $\epsilon(\omega)$  can be analytically continued into the complex  $\omega$  plane [29], in order to compute  $S(\omega)$  for complex  $\omega$ .

Fig. 3(a) shows the poles and zeros for a one-port Fabry-Pérot cavity with this dielectric function. Both the

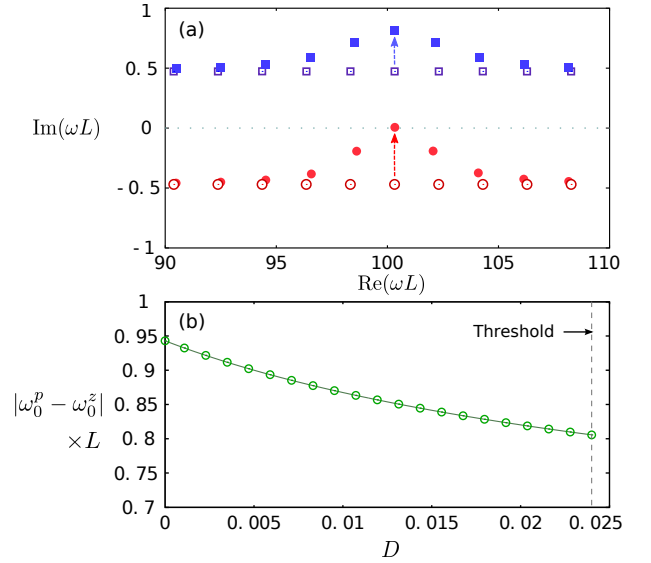


FIG. 3. (color online) (a) Effect of Maxwell-Bloch gain medium on poles and zeros. Poles (circles) and zeros (squares) are plotted for a one-port Fabry-Pérot cavity of length  $L$ , for passive dielectric  $\epsilon = 2.5$  (open symbols) and for a Maxwell-Bloch medium (filled symbols) with  $n_0^2 = 2.5$ ,  $\gamma_{\perp} = 2/L$ ,  $\omega_a = 100.3/L$ , and  $D = 0.024$ . The gain medium moves the poles up by a greater distance than the zeros, resulting in the gain dispersion linewidth correction factor of Ref. 12. (b) Values of  $|\omega_0^p - \omega_0^z|$  for the zero and pole closest to the gain center, versus the pump  $D$ . The dots are exact numerical solutions; the line is an approximation using Eq. (14).

poles and zeros are moved upward, *but the zeros move by a smaller distance*. As a result, in Eq. (6) the leading factor of  $|\omega_0^p - \omega_0^z|$  is smaller than  $\gamma_0$ , and the product terms (which, as discussed above, give rise to the Petermann factor) are likewise reduced.

The fact that the zeros move less than the poles can be understood intuitively from Eq. (12). The effect of the gain medium (which pushes poles and zeros upward in the complex plane) is large when  $\omega$  is close to  $\omega_a - i\gamma_{\perp}$ , which lies in the lower half-plane. Hence the zeros, which are in the upper half plane, “experience less gain” than the poles in the lower half plane. The resulting linewidth reduction can, in principle, overcome the increase due to the Petermann factor, resulting in a linewidth *below* the Schawlow-Townes limit.

The linewidth reduction can be quantified in a simple way for our toy model of a spatially uniform 1D one-port cavity, for which the pole and zero frequencies  $\omega_{p,z}$  are given by Eq. (8). For the passive cavity,  $n = n_0$ , suppose that there is a pair of poles and zeros located at  $\omega_0 \mp i\gamma_0/2$ . For the pumped cavity, the refractive index is  $n = n' + in''$  and the central pole and zero frequencies become  $\omega_{p,z} = \omega'_{p,z} + i\gamma_{p,z}$ . If  $r$  is approximately independent of

$n$  and  $\omega$ , Eq. (8) gives

$$\omega'_{p,z} = \frac{1}{|n|^2} \left[ \mp n_0 n'' \frac{\gamma_0}{2} + n_0 n' \omega_0 \right] \quad (13)$$

$$\gamma_{p,z} = \frac{1}{|n|^2} \left[ \mp n_0 n' \frac{\gamma_0}{2} - n_0 n'' \omega_0 \right]. \quad (14)$$

Threshold occurs when  $n''/n' = \gamma_0/2\omega_0$ . For a high-Q cavity ( $\gamma_0 \ll \omega_0$ ), this implies  $|n''| \ll |n'|$  and  $\omega'_{p,z} \approx \omega_0$ , as expected. Now suppose the medium has the Maxwell-Bloch form, with the gain curve centered on this pair of poles and zeros ( $\omega_a = \omega_0$ ). From Eq. (12), at the pole and zero frequencies,

$$\frac{n''}{n'} \approx -\frac{D\gamma_\perp}{2n_0^2(\gamma_{p,z} + \gamma_\perp)}. \quad (15)$$

Threshold occurs at  $D = n_0^2\gamma_0/\omega_0$ . From Eqs. (14)-(15), we can find the imaginary part of the zero frequency at threshold:

$$\gamma_z = \frac{\gamma_0}{2} \left( 1 + \frac{\gamma_\perp}{\gamma_z + \gamma_\perp} \right) \quad (16)$$

$$= \gamma_0 \left[ 1 + \frac{\gamma_z}{2\gamma_\perp} \left( 1 + \frac{\gamma_z}{2\gamma_\perp} \right)^{-1} \right]^{-1}. \quad (17)$$

Hence,

$$\gamma_z \geq \gamma_0 \left[ 1 + \frac{\gamma_0}{2\gamma_\perp} \right]^{-1}, \quad (18)$$

with the inequality saturating as  $\gamma_0 \ll \gamma_\perp$ . This result is valid for a high-Q cavity at threshold.

The right hand side of (18) is  $\gamma_0$  multiplied by a factor smaller than unity, which is precisely the “bad-cavity” factor previously derived in Refs. 9–12. For the moment, let us consider the perturbative limit,  $\gamma_0 \ll \gamma_\perp$ , where this factor is comparable to unity and the inequality (18) saturates.

For a high-finesse cavity ( $\gamma_0 \ll \Delta\omega$ , occurring for  $|r| \rightarrow 1$ ), the product terms in the ansatz (6) go to unity, so  $\gamma_L \approx \gamma_z$ . In this limit, Eq. (18) gives rise to a laser linewidth which includes a “bad-cavity” factor and a negligible Petermann factor, as expected.

Away from the high-finesse limit ( $\gamma_0 \sim \Delta\omega$ ), the situation is less clear and the Petermann factor cannot be neglected. In the ansatz (6), we must account for the other pairs of poles and zeros, which are located away from the gain center  $\omega_a$ . For example, Fig. 3(a) shows the poles and zeros for a medium-finesse Fabry-Pérot cavity with  $\gamma_0 \approx 0.5\Delta\omega$ . The non-central poles and zeros are displaced upwards from their passive-cavity frequencies, but by less than the central pair. They also experience “line-pulling” towards the gain center  $\omega_a$ . Both effects modify the Petermann factor. The first tends to suppress  $K$ , while the second tends to enhance it. Let us compare  $\sqrt{K_{\text{ansatz}}}$ , as calculated from Eq. (7) with the Maxwell-Bloch gain medium, to the value  $\sqrt{K_0}$  for

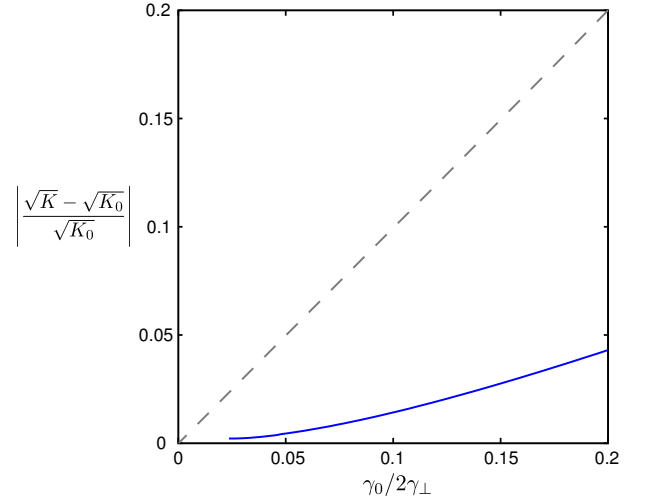


FIG. 4. (color online) Fractional deviation in  $\sqrt{K}$  caused by finite Maxwell-Bloch gain width  $\gamma_\perp$ , as a function of  $\gamma_0/2\gamma_\perp$  (where  $\gamma_0$  is the passive cavity decay rate). This plot is obtained varying  $\gamma_\perp$  in the one-port Fabry-Pérot cavity of Fig. 3, and calculating the Petermann factor from Eq. (7), based on the pole and zero frequencies at threshold. The broad-band limit of the Petermann factor,  $K_0$ , is computed from Eq. (9).

“infinitely broad-band” gain, which is given by Eq. (9). Fig. 4 shows the value of

$$\left| \frac{\sqrt{K_{\text{ansatz}}} - \sqrt{K_0}}{\sqrt{K_0}} \right|$$

versus  $\gamma_0/2\gamma_\perp$ , as  $\gamma_\perp$  is varied in the Fabry-Pérot cavity. It turns out that the effects of gain reduction and line pulling on the Petermann factor cancel to first order leaving a correction which is second-order in  $\gamma_0/2\gamma_\perp$ . Hence, even if the Petermann factor itself is non-negligible, the correction to it due to a finite  $\gamma_\perp$  are negligible compared to the correction to  $\gamma_z$ . The bad-cavity factor and the Petermann factor can be taken to be independent, in the limit  $\gamma_0 \ll \gamma_\perp$ .

Away from the  $\gamma_0 \ll \gamma_\perp$  limit, the inequality (18) does not saturate, and the “bad-cavity” linewidth reduction effect has a significant contribution from the positions of the non-central poles and zeros. In this case, the bad-cavity and Petermann factor cannot be cleanly identified with the leading and product terms in the ansatz (6). In the next section, we will derive a general linewidth formula in terms of the lasing wavefunction, which is valid even if  $\gamma_0 \sim \gamma_\perp$ . We will then show that the bad-cavity correction appears as a separate multiplicative factor, consistent with Refs. 9–12, only for the special case of a Fabry-Pérot cavity. In general the Petermann and bad-cavity factors cannot be separated when  $\gamma_0 \gtrsim \gamma_\perp$ , i.e. in the full bad-cavity regime.

#### IV. WAVEFUNCTION FORMULATION

The generalized decay rate  $\gamma_L$ , defined in Eq. (2), can be re-expressed in terms of the wavefunction of the lasing mode and the frequency-dependent dielectric function of the laser medium. This derivation, which uses a modification of the approximation scheme of Schomerus [26], yields a generalization of the usual Petermann formula (3) that also incorporates the bad-cavity factor. Pick *et al.* have independently derived a similar result, using a coupled mode theory approach which also yields a generalization of the Henry  $\alpha$  factor [30].

Consider a 1D or 2D transverse magnetic (TM) system lasing at a real frequency  $\omega = \omega_0$ . The laser mode is described by a purely-outgoing wavefunction  $\psi_0$  (representing the out-of-plane component of the complex electric field), which satisfies the Helmholtz equation:

$$\begin{aligned} \left[ \nabla^2 + \epsilon(r, \omega_0) \omega_0^2 \right] \psi_0(r) &= 0, \\ \psi_0(r) &= \sum_{\mu} b_{\mu} u_{\mu}(r; \omega_0) \text{ for } r \notin C. \end{aligned} \quad (19)$$

Here,  $C$  denotes the scattering region, and  $\{u_{\mu}\}$  is an appropriate set of outgoing channel modes defined in the region outside  $C$ , where  $\epsilon = 1$ . For open 2D geometries, it is convenient to let  $C$  be a circle of radius  $R$ , and define

$$u_{\mu}(r, \phi; \omega) = \frac{H_{\mu}^{+}(\omega r)}{\sqrt{R} H_{\mu}^{+}(\omega R)} \Phi_{\mu}(\phi), \quad (20)$$

with azimuthal basis functions satisfying  $\int_0^{2\pi} d\phi \Phi_{\mu} \Phi_{\nu} = \delta_{\mu\nu}$ . The vector  $\mathbf{b} = [b_1, \dots]$  is an eigenvector of  $S(\omega_0)$ , with diverging eigenvalue.

Next, consider a frequency  $\omega$  differing slightly from  $\omega_0$ . The  $S$ -matrix remains dominated by the pole, so [26]

$$S(\omega) \approx \frac{\sigma(\omega)}{\mathbf{b}^T \mathbf{b}} \mathbf{b} \mathbf{b}^T, \quad (21)$$

with  $\sigma(\omega)$  finite. Let  $\mathbf{a}$  be an input amplitude, normalized so that the output amplitude is equal to  $\mathbf{b}$ . From (21), the generalized decay rate is

$$\gamma_L = \left| \text{Res} \left[ \sigma(\omega) \frac{\mathbf{b}^{\dagger} \mathbf{b}}{\mathbf{b}^T \mathbf{b}} \right] \right| = \mathbf{b}^{\dagger} \mathbf{b} \left| \text{Res} \left( \frac{1}{\mathbf{b}^T \mathbf{a}} \right) \right|, \quad (22)$$

with the residue evaluated in the limit  $\omega \rightarrow \omega_0$ . The corresponding wavefunction,  $\psi(r)$ , obeys

$$\begin{aligned} \left[ \nabla^2 + \epsilon(r, \omega) \omega^2 \right] \psi(r) &= 0, \\ \psi(r) &= \sum_{\mu} [a_{\mu} u_{\mu}^{*}(r) + b_{\mu} u_{\mu}(r)] \text{ for } r \notin C. \end{aligned} \quad (23)$$

According to Gauss's theorem,

$$\begin{aligned} \int_C d^d r \left[ \psi_0 \nabla^2 \psi - \psi \nabla^2 \psi_0 \right] &= \left[ \psi_0 \nabla \psi - \psi \nabla \psi_0 \right]_{\partial C} \\ &= -i(\omega + \omega_0) \mathbf{b}^T \mathbf{a} + i(\omega - \omega_0) \mathbf{b}^T \mathbf{b}. \end{aligned} \quad (24)$$

The final equality in (24) is exact for 1D, and approximate for the 2D modes defined in (20) in the limit  $\omega R \gg 1$ . From the wave equation, (24) also equals

$$\begin{aligned} \int_C d^d r \left[ \epsilon(r, \omega_0) \omega_0^2 - \epsilon(r, \omega) \omega^2 \right] \psi_0 \psi \\ \approx -(\omega - \omega_0) \int_C d^d r \left[ \omega^2 \frac{d\epsilon}{d\omega} + 2\epsilon \omega \right]_{\omega_0} \psi_0^2. \end{aligned} \quad (25)$$

Exploiting the time reversal symmetry of the Helmholtz equation,  $\psi_0^*$  acts as a purely incoming solution with  $\epsilon \rightarrow \epsilon^*$ . This gives

$$\begin{aligned} \int_C d^d r \left[ \psi_0 \nabla^2 \psi_0^* - \psi_0^* \nabla^2 \psi_0 \right] &= \left[ \psi_0 \nabla \psi_0^* - \psi_0^* \nabla \psi_0 \right]_{\partial C} \\ &= -i(\omega_0^* + \omega_0) \mathbf{b}^{\dagger} \mathbf{b}, \end{aligned} \quad (26)$$

and using the wave equation as before,

$$\begin{aligned} \int_C d^d r \left[ \epsilon(r, \omega_0) \omega_0^2 - \epsilon^*(r, \omega_0) (\omega_0^*)^2 \right] |\psi_0|^2 \\ = \int_C d^d r 2 \text{Im}[\epsilon(r, \omega) \omega_0^2] |\psi_0|^2. \end{aligned} \quad (27)$$

Combining these equations and using (22) yields

$$\gamma_L = \frac{\omega_0 \int_C d^d r \text{Im}[\epsilon(r, \omega_0) \omega_0^2] |\psi_0|^2}{\text{Re}(\omega_0) \left[ \frac{i \mathbf{b}^T \mathbf{b}}{2} + \int_C d^d r \left[ \epsilon \omega + \frac{\omega^2}{2} \frac{d\epsilon}{d\omega} \right]_{\omega_0} \psi_0^2 \right]}. \quad (28)$$

Eq. (28) expresses the generalized cavity decay rate in terms of the lasing mode (19), valid for arbitrary cavity geometries and gain media. We now show that it reduces to the usual bad-cavity linewidth formula for the special case of a uniform 1D Fabry-Pérot cavity of length  $L$ . The  $\mathbf{b}^T \mathbf{b}/2$  term in the denominator is normalized to the value of  $\psi(r)$  at the cavity boundary, in accordance with Eq. (23). We will drop this term, as it is negligible for  $\omega_0 L \gg 1$ . For  $\omega_0 = \text{Re}(\omega_0)$ , Eq. (28) becomes

$$\gamma_L = B \sqrt{K} \gamma_0, \quad (29)$$

where

$$B = \left| 1 + \frac{\omega}{2\epsilon} \frac{d\epsilon}{d\omega} \right|_{\omega_0}^{-1} \quad (30)$$

$$K = \left| \frac{\int dz |\psi_0|^2}{\int dz \psi_0^2} \right|^2 \quad (31)$$

$$\gamma_0 = -\frac{\omega_0 \text{Im}[\epsilon(\omega_0)]}{|\epsilon(\omega_0)|} \quad (32)$$

are respectively the bad-cavity factor, the longitudinal Petermann factor [6], and the passive cavity decay width.



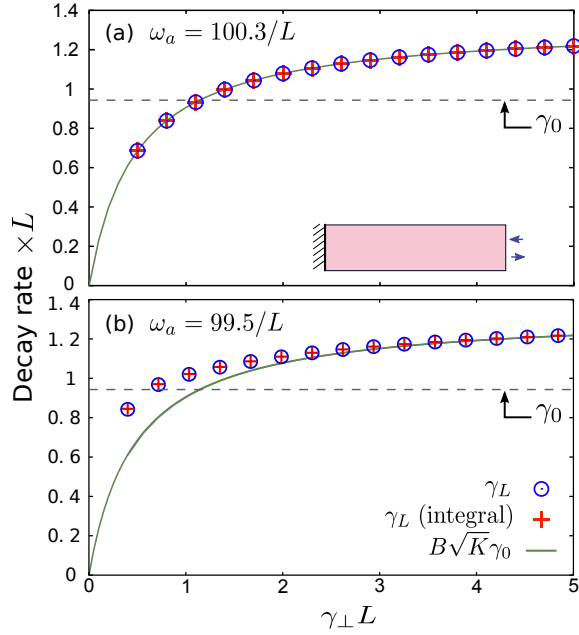


FIG. 5. (color online) Generalized decay rates for a one-port Fabry-Pérot laser at threshold, versus the gain width  $\gamma_{\perp}$ . The Maxwell-Bloch gain medium has background permittivity  $n_0^2 = 2.5$ , with the pump adjusted so that the laser is at threshold. Results are shown for (a)  $\omega_a = 100.3/L$ , centered on one of the poles of the passive cavity; and (b)  $\omega_a = 99.5/L$ , detuned from the pole by slightly less than a free spectral range. In both plots, the decay rates are calculated using the exact formula for  $\gamma_L$  from Eq. (2) (blue circles), using the integral approximation (28) (red crosses), and using the Fabry-Pérot-specific Eqs. (29)-(32) (solid line). The passive cavity decay rate  $\gamma_0$  is also shown (dashed line).

In (32),  $\gamma_0$  was identified via the standard relation between the passive cavity resonance frequency  $\omega_c$  and the lasing refractive index  $n_0$  in a Fabry-Pérot cavity [28]:

$$\frac{\text{Im}(n_0)}{\text{Re}(n_0)} = \frac{\text{Im}(\epsilon)}{2\text{Re}(\epsilon)} \approx \frac{\text{Im}(\omega_c)}{\text{Re}(\omega_c)} \approx -\frac{\gamma_c/2}{\omega_0}. \quad (33)$$

This approximation assumes that line-pulling is negligible. We now focus on the  $B$  factor of Eq. (30). Using the Maxwell-Bloch dielectric function (12) in the limit  $\omega_a \approx \omega_0 \gg \gamma_{\perp}$ , together with Eq. (33), Eq. (30) simplifies to

$$B \approx \left| 1 + \frac{\omega_0 D}{2n_0^2 \gamma_{\perp}} \right|^{-1} \approx \left| 1 + \frac{\gamma_c}{2\gamma_{\perp}} \right|^{-1}. \quad (34)$$

The above results are verified numerically in Fig. 5, for one-port Fabry-Pérot lasers at threshold (with varying  $\gamma_{\perp}$ ). The  $S$ -matrix theory is typically in good agreement with the Fabry-Pérot specific Eqs. (29)-(32). Discrepancies are, however, observed when  $\omega_a$  is significantly detuned from a lasing pole and  $\gamma_{\perp}$  is small, as shown in Fig. 5(b). In this regime, the lasing modes are strongly affected by line-pulling, so that the factorization (29) breaks down. In all the studies we have performed, the

integral form of the generalized decay rate, Eq. (28), is in excellent agreement with  $\gamma_L$  as evaluated directly from the  $S$ -matrix. It should be noted that both approaches require solving the SALT equations for the (in general) non-linear multimode lasing state, but once that is done the integral formula is evaluated simply by performing the relevant integrals of SALT solutions over the lasing cavity, whereas the  $S$ -matrix residue formula typically requires more involved calculations.

The key approximations (21) and (24)-(27) were previously used by Schomerus to derive a generalization of the Petermann factor for 2D lasers [26]. The method of Schomerus differs from ours in several respects. Instead of calculating the  $S$ -matrix eigenvalue residue, he calculated the amplified spontaneous emission (ASE) intensity,

$$I(\omega) \approx \frac{1}{2\pi} \text{Tr}(S^\dagger S) \approx \frac{1}{2\pi} \left| \frac{\mathbf{b}^\dagger \mathbf{b}}{\mathbf{b}^\dagger \mathbf{a}} \right|^2, \quad (35)$$

for a *sub-threshold* laser cavity. In Eqs. (24)-(25), the wavefunction  $\psi$  is chosen to be that of the sub-threshold system, whose dielectric function  $\epsilon$  differs from the threshold laser's dielectric function  $\epsilon_L$ . For real  $\omega$ , Eq. (35) gives a Lorentzian with width  $\Delta\omega$ , inverse to the total ASE power  $P = \hbar\omega_0 \int I(\omega) d\omega$ ; this Schawlow-Townes-like relationship is argued to hold as the system approaches threshold, at which point it becomes the laser linewidth. Furthermore,  $I(\omega)$  diverges at a complex frequency below the real- $\omega$  axis, corresponding to the pole of the sub-threshold cavity. By assuming that Eq. (35) holds all the way down to the passive cavity limit, where the dielectric function is  $\approx \text{Re}(\epsilon_L)$  and the resonance frequency is  $\approx \omega_0 - i\gamma_0/2$ , Schomerus obtains [26]

$$\Delta\omega \approx \frac{\hbar\omega_0\gamma_0^2}{P_{\text{tot}}} \left| \frac{\int d^2r \text{Im}(\epsilon_L) |\psi_0|^2}{\int d^2r \text{Im}(\epsilon_L) \psi_0^2} \right|^2. \quad (36)$$

Note that this reduces to the traditional formula for the longitudinal Petermann factor for uniform cavities.

Thus, in Schomerus' theory the relevant approximations are based on a perturbation between a passive cavity pole and a lasing pole. By contrast, we have used the approximation (25) to describe a truly infinitesimal deviation from an  $S$ -matrix pole, for the purpose of extracting the residue of the pole. As might be expected, the Schomerus result (36) agrees well with our present theory when  $\gamma_0$  is much smaller than all other frequency scales, including  $\gamma_{\perp}$  and the free spectral range. However the two do not agree in other regimes, when dispersion is non-negligible, since the frequency dependence of  $\epsilon$  is ignored. In the next section we will correct the Schomerus theory by including the traditional bad-cavity factor (18) by hand and use this hybrid theory to compare to our more complete theory for complex cavities.

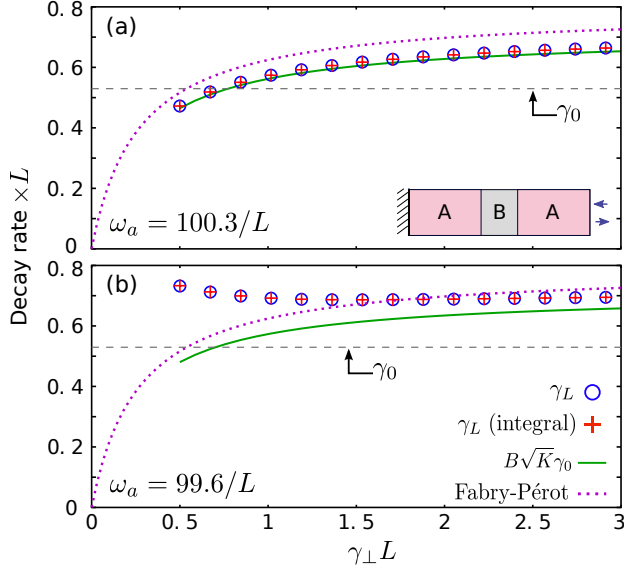


FIG. 6. (color online) Generalized decay rates versus gain width  $\gamma_{\perp}$ , for a partially-pumped non-uniform laser at threshold with the gain centers (a)  $\omega_a = 100.3/L$  and (b)  $\omega_a = 99.6/L$ . The laser consists of three slabs of lengths  $[0.4L, 0.2L, 0.4L]$  (inset schematic). The A slabs contain gain material with background  $n_0^2 = 2.25$ ; the B slab has passive  $\epsilon = 9$ . The generalized decay rate  $\gamma_L$  is computed from the  $S$ -matrix (blue circles), and from the integral approximation Eq. (28) (red crosses). The solid curves show the traditional result  $B\sqrt{K}\gamma_c$ , where  $B$  is the bad-cavity factor of Eq. (30) and  $K$  is the Petermann factor of Eq. (36). The dotted curves show the result for a uniform Fabry-Pérot cavity with region  $B$  replaced with gain material.

## V. COMPLEX LASER CAVITIES

Having established that the  $S$ -matrix theory agrees analytically and numerically with previous theories for uniform 1D lasers, we now turn to more complex cases—1D lasers with spatially non-uniform dielectric functions and pumping, 2D lasers, and the effect of spatial hole-burning above threshold.

Fig. 6 shows the variation of  $\gamma_L$  with  $\gamma_{\perp}$ , at threshold, for a non-uniform 1D laser with spatially inhomogeneous dielectric function and pumping. Over the entire computed range, the integral formula (28) is again in excellent agreement with the exact  $\gamma_L$  computed from the  $S$ -matrix. To compare our  $S$ -matrix or SALT integral results for more general cavities to the most complete version of the “traditional” results, we combine the Schome-rus formula, Eq. (36), with an *ad hoc* bad-cavity factor. If we do this, good agreement is observed in Fig. 6(a), when the gain center  $\omega_a$  is aligned with one of the passive cavity resonances and line-pulling is negligible. In Fig. 6(b), a different choice of  $\omega_a$  introduces line-pulling, and the  $S$ -matrix theory gives significantly different results, particular for small values of  $\gamma_{\perp}$ .

Fig. 7 shows an analogous two-dimensional calculation,

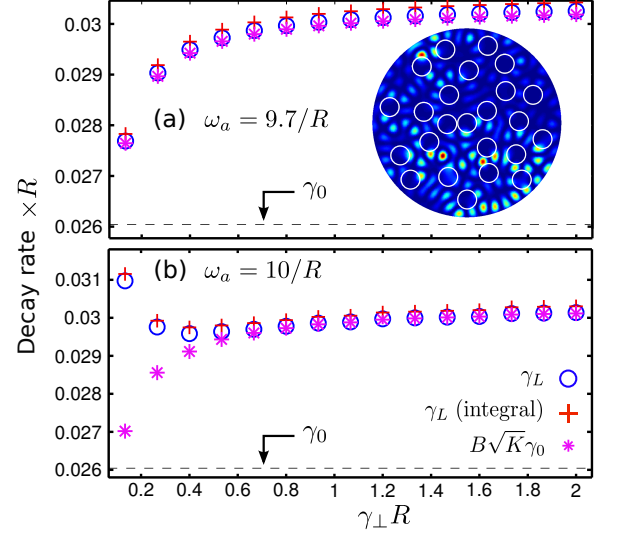


FIG. 7. (color online) Generalized decay rates versus gain width  $\gamma_{\perp}$ , for a two-dimensional random laser at threshold. The laser cavity consists of a pumped dielectric disk of radius  $R = 1$ , background dielectric  $n_0^2 = 10$ , with 24 randomly-placed air holes of radius 0.1. The wave equation is solved by the finite-element method, and the generalized decay rate  $\gamma_L$  is computed from the  $S$ -matrix (blue circles) and from the integral approximation Eq. 28 (red crosses). The result of the traditional formula  $B\sqrt{K}\gamma_c$  is shown for comparison (magenta asterisks), where  $K$  is computed from the Schome-rus formula of Eq. 36. Two values of the gain center are used: (a)  $\omega_a = 9.7$ , for which the lasing mode has negligible line-pulling, and (b)  $\omega_a = 10$ . Inset: Computed mode intensity for the threshold lasing mode.

for a random laser cavity. Again, good agreement is observed between the exact  $\gamma_L$  and the integral formula. The  $S$ -matrix theory approaches the traditional result for large values of  $\gamma_{\perp}$  and negligible-line-pulling, and by more than 10% for small values of  $\gamma_{\perp}$ . This is consistent with the results found in 1D.

As described in Ref. 21,  $\gamma_L$  can be computed above the lasing threshold by using the nonlinear  $S$ -matrix. Above threshold,  $\epsilon(r)$  is modified by spatial hole burning; instead of being an independent parameter, the inversion  $D$  in Eq. (12) becomes [22–25]

$$D(r) = D_0 F(r) \left[ 1 + \sum_{\nu} \Gamma_{\nu} |\Psi(r)|^2 \right]^{-1}, \quad (37)$$

$$\Gamma_{\nu} \equiv \frac{\gamma_{\perp}^2}{\gamma_{\perp}^2 + (k_{\nu} - k_a)^2},$$

where  $D_0$  is the pump strength,  $F(r)$  is the spatial profile of the pump (which is zero in unpumped regions), and  $k_{\nu}$  and  $\Psi_{\nu}(r)$  are the self-consistently determined frequency and field function of the  $\nu$ -th lasing mode (the possibility of multi-mode lasing is thus explicitly included). The resulting complex  $\epsilon(r)$  enters into the linewidth theory in exactly the same way as at threshold: we can obtain



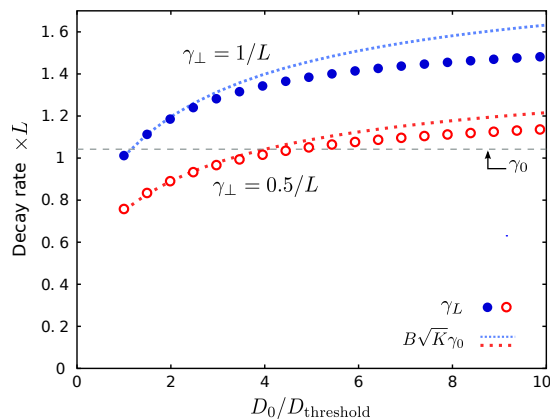


FIG. 8. (color online) Generalized decay rates for above-threshold lasers. The laser cavity is a slab of length  $L$  with a perfect reflector on one side. The gain medium is uniformly pumped, with parameters  $n_0^2 = 2.3$  and  $\omega_a = 100.3/L$  as described via Eqs. (12) and (37). The pump  $D_0$  is varied from the threshold value up to  $10\times$  threshold. The values of  $\gamma_L$  are shown for gain widths of  $\gamma_\perp = 1/L$  (filled circles) and  $\gamma_\perp = 0.5/L$  (open circles). The dotted lines show the corresponding values of  $B\sqrt{K}\gamma_c$ , where  $B$  is the bad-cavity factor and  $K$  is the Petermann factor of Eq. (36). For these parameters, the laser is single-mode.

the  $S$ -matrix and hence  $\gamma_L$ , or obtain  $\Psi_\nu(r)$  and use it directly in the integral formula (28).

Fig. 8 shows  $\gamma_L$  as a function of  $D_0$  for a 1D Fabry-Pérot cavity. The value of  $\omega_a$  is chosen so that, at threshold, there is negligible line-pulling; hence the  $S$ -matrix and traditional results are in good agreement (as discussed above). As the pump is increased, the results begin to deviate, up to 4% at a pump of  $10\times$  threshold. Comparing this to the results of Ref. 21, we conclude that the deviations from the Schawlow-Townes-Petermann linewidth formula discussed in that paper was due to the bad-cavity factor. However, Fig. 8 also shows deviations at large pump strengths, which cannot be explained by the bad-cavity factor.

In Fig. 8, the variation in the decay rate with respect to the pump can be intuitively linked to the motion of

the poles and zeros by using Eq. (6). Suppose that we have a single lasing mode at threshold. This corresponds to a pole sitting on the real frequency axis. As the pump is increased, other poles and zeros, including the zero associated with the lasing pole, continue to move up the complex frequency plane. The lasing pole however remains stationary on the real frequency axis. As a result, both the prefactor and product terms in Eq. (6), and hence  $\gamma_L$ , increase with pump,  $D_0$ . As the pump is further increased, a second mode turns on and the motions of the other poles and zeros slow down. This causes the terms in Eq. (6) to remain relatively constant as  $D_0$  increases. Thus,  $\gamma_L$  increases more slowly with  $D_0$ .

In conclusion, we have found that the  $S$ -matrix theory of the laser linewidth incorporates both the bad-cavity linewidth reduction factor and the Petermann factor. For simple cavities, particularly uniform Fabry-Pérot cavities with negligible line pulling and close to threshold, the bad-cavity and Petermann factors can be treated as independent quantities. In such systems, we obtain results that are consistent both with the studies of the bad-cavity factor in Refs. 9–14, and with Schomerus’ generalization of the Petermann factor, without the bad-cavity factor, in Ref. 26. On the other hand, in the most general case the bad-cavity and Petermann effects do not emerge as independent factors, as we saw in Eq. (28) when expressing the generalized cavity decay rate in terms of the lasing wavefunction; this was confirmed in numerical examples with strong line-pulling and spatial hole-burning. In future work, these deviations will be studied further, with the goal of developing experimentally feasible laser systems with anomalous linewidth behaviors.

## VI. ACKNOWLEDGMENTS

We would like to thank A. Cerjan, S. G. Johnson, A. Pick, and S. Rotter for helpful discussions. This research was supported by the Singapore National Research Foundation under grant No. NRFF2012-02 and by NSF grant DMR-1307632.

- 
- [1] A. L. Schawlow and C. H. Townes, Phys. Rev. **112** 1940 (1958).
  - [2] K. Petermann, IEEE J. Quant. Elect. **15**, 566 (1979).
  - [3] H. Haus and S. Kawakami, IEEE J. Quant. Elect. **21**, 63 (1985).
  - [4] C. H. Henry, J. Lightwave. Tech. **LT-4**, 288 (1986).
  - [5] A. E. Siegman, Phys. Rev. A **39**, 1253 (1989); **39**, 1264 (1989).
  - [6] W. A. Hamel and J. P. Woerdman, Phys. Rev. A **40**, 2785 (1989).
  - [7] W. A. Hamel and J. P. Woerdman, Phys. Rev. Lett **64**, 1506 (1990).
  - [8] C. H. Henry, IEEE J. Quant. Elect. **18**, 259 (1982).
  - [9] M. Lax, in *Physics of Quantum Electronics*, edited by P. L. Kelley, B. Lax, and P. E. Tannenwald (McGraw-Hill, New York, 1966), p.735.
  - [10] H. Haken, *Laser Theory* (Springer, Berlin, 1984).
  - [11] M. I. Kolobov, L. Davidovich, E. Giacobino, and C. Fabre, Phys. Rev. A **47**, 1431 (1993).
  - [12] M. P. van Exter, S. J. M. Kuppens, and J. P. Woerdman, Phys. Rev. A **51**, 809 (1995).
  - [13] S. J. M. Kuppens, M. P. van Exter, and J. P. Woerdman, Phys. Rev. Lett. **72**, 3815 (1994).
  - [14] S. J. M. Kuppens, M. P. van Exter, M. van Duin, and J. P. Woerdman, IEEE J. Quant. Elect. **31**, 1237 (1995).

- [15] D. Meiser, J. Ye, and M. J. Holland, New J. Phys. **10**, 073014 (2008).
- [16] D. Meiser, J. Ye, D. R. Carlson, and M. J. Holland, Phys. Rev. Lett. **102**, 163601 (2009).
- [17] D. Meiser and M. J. Holland, Phys. Rev. A **81**, 033847 (2010).
- [18] D. Meiser and M. J. Holland, Phys. Rev. A **81**, 063827 (2010).
- [19] J. G. Bohnet *et al.*, Nature **484**, 78 (2012).
- [20] T. Liu, K. E. Lee, and Q. J. Wang, Opt. Ex. **20**, 17145 (2012).
- [21] Y. D. Chong and A. D. Stone, Phys. Rev. Lett. **109**, 063902 (2012).
- [22] H. E. Türeci, A. D. Stone, and B. Collier, Phys. Rev. A **74**, 043822 (2006).
- [23] H. E. Türeci, A. D. Stone, and L. Ge, Phys. Rev. A **76**, 013813 (2007).
- [24] H. E. Türeci, L. Ge, S. Rotter, and A. D. Stone, Science **320**, 643 (2008).
- [25] L. Ge, Y. D. Chong, and A. D. Stone, Phys. Rev. A **82**, 063824 (2010).
- [26] H. Schomerus, Phys. Rev. A **79**, 061801(R) (2009).
- [27] Y. D. Chong, H. Cao, and A. D. Stone, Phys. Rev. A **87**, 013843 (2013).
- [28] Y. D. Chong, L. Ge, H. Cao and A. D. Stone, Phys. Rev. Lett. **105**, 053901 (2010).
- [29] J. S. Toll, Phys. Rev. **104**, 1760 (1956).
- [30] A. Pick *et al.*, manuscript in preparation.